View Article Online / Journal Homepage / Table of Contents for this issue
Dynamic Article Links

RSC Advances

Cite this: *RSC Advances*, 2012, **2**, 7569–7577

www.rsc.org/advances

PAPER

Morphology-controllable synthesis and enhanced luminescence properties of β-$NaLuF_4$:Ln (Ln = Eu, Tb and Ce/Tb) microcrystals by solvothermal process†

Fei He,[a] Na Niu,[a] Zhenguo Zhang,[b] Xiao Zhang,[a] Dong Wang,[a] Ling Bai,[a] Shili Gai,[a] Xingbo Li[a] and Piaoping Yang*[a]

Received 13th April 2012, Accepted 11th June 2012
DOI: 10.1039/c2ra20675g

Published on 13 June 2012. Downloaded on 21/01/2016 08:21:03.

Controlled synthesis of β-$NaLuF_4$ with uniform morphology, dimension and considerable monodispersity was designed *via* a gentle solvothermal process by using ethylenediamine (EDA) and ethylene glycol (EG) as the mixed solvent and $NaNO_3$ as a mineralizer. X-ray diffraction (XRD), field scanning electron microscopy (FESEM), transmission electron microscopy (TEM), high-resolution transmission electron microscopy (HRTEM), energy dispersive X-ray spectra (EDS) and down-conversion (DC) photoluminescence spectra were used to characterize the samples. The results indicate that the as-prepared β-$NaLuF_4$ microcrystals can be rationally modified in phase, size and morphology by tuning the solvent constitution, $NaNO_3$ content, and reaction time. Moreover, the crystal growth process was thoroughly discussed through a series of time-dependent experiments and a possible formation mechanism was proposed. Furthermore, the DC luminescence properties as well as the emission mechanisms of β-$NaLuF_4$:Ln^{3+} (Ln = Eu, Tb and Ce/Tb) microcrystals were systematically investigated. It is found that the DC luminescence properties can be improved observably by introducing Ce^{3+} into the β-$NaLuF_4$ microcrystals and the doping concentration of the Ce^{3+} is optimized under a fixed concentration of Tb^{3+}. It is expected that the synthesis strategy can be applied to prepare many other types of micro- and nano-crystals as well.

1. Introduction

In the field of modern materials science and technology, control over crystallization remains the key issue and research focus, due to its potential applications in the preparation of well-defined crystals with uniform shapes and assembly of building blocks into ordered superstructures.[1–6] To date, several approaches have been employed to synthesize nano- and microcrystals (NCs and MCs) with uniform phase, dimension and morphology, such as the solid-state combinatorial chemistry method,[7,8] the molten-salt approach,[9] hydrothermal and solvothermal techniques,[10–13] the sol–gel route,[14,15] and chemical vapor synthesis.[16] In particular, as a typical representative of the solution-based approach, the solvothermal method has proved to be an effective and convenient approach in the precise architectural manipulation of inorganic functional materials with well-defined morphologies and accurately adjustable sizes.[17–21] In fact, the solvent under different conditions can not only play a role as the surrounding guest of the reaction, but also chelate with the reactant as a ligand and thus direct the evolution of the structure and morphology of the products. Furthermore, under solvothermal conditions, many starting materials can undergo quite unexpected reactions, which are often accompanied by the formation of nanoscopic morphologies that are not accessible by classical routes. For example, Qian's group synthesized ultra-long Bi_2S_3 nanoribbons with lengths of up to a few millimeters *via* a solvothermal method using an aqueous NaOH solution and glycerol as the solvent.[22] Yang *et al.* demonstrated a solvothermal route for the synthesis of high-quality anatase TiO_2 single crystals by using 2-propanol as a synergistic capping agent and reaction medium.[23] Recently, a solvothermal reduction method has been developed to decrease the number of defects and the oxygen content in graphene sheets and graphite oxide.[24] An EDA-assisted solvothermal reaction in an EG solvent has been adopted to fabricate some advanced materials,[25,26] where the EG and EDA acted as synergic effects in the solvothermal system to direct the crystal growth process. However, to the best of our knowledge, controlled preparation of luminescent rare-earth fluorides through the EG-EDA solvothermal method has never been reported.

In the past two decades, rare-earth based materials have attracted much research interest because of their novel electronic and optical properties resulting from their 4f electrons.[27–31] Among the various rare earth phosphors, β-$NaREF_4$ has

[a]*Key Laboratory of Superlight Materials and Surface Technology, Ministry of Education, Harbin Engineering University, Harbin, 150001, P. R. China. E-mail: yangpiaoping@hrbeu.edu.cn*
[b]*College of Science, Harbin Engineering University, Harbin, 150001, P. R. China*

† Electronic Supplementary Information (ESI) available. See DOI: 10.1039/c2ra20675g

View Article Online

Published on 13 June 2012. Downloaded on 21/01/2016 08:21:03.

received more and more attention for its enormous potential applications in diverse fields, such as solid-state lasers,[32,33] 3D flat-panel displays,[34,35] biological detection,[36,37] low-intensity IR imaging,[38] sensing[39] and so forth. Particularly, β-$NaLuF_4$ nano- and microcrystals have been regarded as excellent host lattices for the down-conversion (DC) and up-conversion (UC) luminescence of lanthanide ions.[40,41] In comparison with Y^{3+}, Lu^{3+} may be more favorable for trivalent lanthanide (Ln^{3+}) dopant emission due to the intensity-borrowing mechanism mixing the 4f and 5d orbitals of the Ln^{3+} ions *via* the lattice valence band level.[42,43] Moreover, Lu^{3+} ion doping can also influence the population life time of the emitters, which may, remarkably, tune the luminescence properties (*e.g.* brightness and long afterglow performance).[44,45] However, from previous research, there are always several different excitation points in the DC emission of β-$NaLuF_4$:Ln (Ln = Eu^{3+}, Tb^{3+}) phosphors, which means a relatively low energy transfer efficiency and inconvenience for further applications.[41] Recently, several groups doped Ce^{3+} as the sensitizer in combination with other lanthanide ions as corresponding activators,[46–49] which may provide an effective method to solve this problem. From the viewpoint of energy transfer, Ce^{3+} and Ln co-doped phosphors may generate light more efficiently.[50] However, this kind of energy transfer process in the β-$NaLuF_4$ host lattice has rarely been reported so far.

Accordingly, in the present work, we propose a template-free, no-seed solvothermal process for the synthesis of uniform Ln^{3+} (Ln = Eu, Tb and Ce/Tb) doped β-$NaLuF_4$ MCs with high monodispersity. Ethylene glycol (EG) and ethylenediamine (EDA) was chosen as the solvent in the reaction system to govern the morphology, size and dimension of the products. The effects of the solvent constitution (volume ratio of EG to EDA), $NaNO_3$ content in the initial solution and reaction time on the crystal dimension, structure and morphology have been investigated in detail. It can be found that the size, structure, and morphology of the products can be precisely controlled by modulation of the conditions above, and a possible mechanism of crystal growth has also been proposed. Additionally, the DC luminescence properties of Eu^{3+}, Tb^{3+} and Ce^{3+}/Tb^{3+} doped β-$NaLuF_4$ MCs have been thoroughly studied.

2. Experimental section

2.1. Materials

All materials including analytical grade $NaNO_3$, $Ce(NO_3)_3{\cdot}6H_2O$, ethylene glycol (EG) and ethylenediamine (EDA) were purchased from Sinopharm Chemical Reagent Co., Ltd and used as received without further purification. $Lu(NO_3)_3$, $Eu(NO_3)_3$ and $Tb(NO_3)_3$ were prepared by dissolving the corresponding Lu_2O_3, Eu_2O_3, and Tb_4O_7 (99.99%, Sinopharm Chemical Reagent Co., Ltd, China) in HNO_3 solution at elevated temperature followed by evaporating the superfluous HNO_3 and the solvent under vacuum.

2.2. Preparation of β-$NaLuF_4$

All of the doping ratios of Ln^{3+} are molar in our experiments. In a typical procedure for the preparation of β-$NaLuF_4$:5% Ce^{3+}/2.5% Tb^{3+} MCs, 0.925 mmol $Lu(NO_3)_3$, 0.05 mmol $Ce(NO_3)_3$, 0.025 mmol $Tb(NO_3)_3$ and 2.5 mmol (0.1 g) $NaNO_3$ were dissolved in a mixed solvent composed of 3 mL EG and 7 mL EDA under ultrasonication. Afterwards, a solution of 12.5 mmol NH_4F in 10 mL EDA was added into the above solution under vigorous stirring. After stirring for 30 min, the mixed solution was transferred into a Teflon bottle of volume 30 mL in a stainless steel autoclave, sealed, and maintained at 200 °C for 48 h. As the autoclave cooled to room temperature naturally, the precipitates were separated by centrifugation, washed with deionized water and ethanol in sequence, and then dried in air at 70 °C for 12 h. $NaLuF_4$:2.5% Eu^{3+}, $NaLuF_4$:2.5% Tb^{3+} and $NaLuF_4$:*x*% Ce^{3+}/2.5% Tb^{3+} (*x* = 2.5, 7.5, 10) samples were prepared in a manner similar to that of β-$NaLuF_4$:5% Ce^{3+}/2.5% Tb^{3+}. Different solvent constitution (volume ratio of EG/EDA = 0 : 20, 3 : 17, 7 : 13, 10 : 10, 13 : 7, 17 : 3 and only EG as the solvent), differing $NaNO_3$ content (5, 7.5, 10 mmol), different mineralizers (Na_2SO_4, Na_3PO_4) and time-dependent experiments (reaction time = 1, 3, 6 h) were employed to study the effects on the morphology, structure and size of the as-synthesized products. It should be pointed out that, when the effect of one reaction condition was studied, the other reaction conditions were kept the same as those for the typical fabrication.

X-ray diffraction (XRD) was examined on a Rigaku-Dmax 2500 diffractometer using Cu-Kα radiation (λ = 0.15405 nm). The XRD samples are prepared by putting the absolute dry $NaLuF_4$ powder on a glass slide substrate and pressed lightly with another glass slide. Analysis of the composition of the metallic elements was performed using inductively coupled plasma (ICP) emission spectroscopy on a Thermal XSeries II in solutions prepared by dissolving the samples in dilute HNO_3. The morphology and composition of the as-prepared samples were inspected on a field emission scanning electron microscope (FESEM, S4800, Hitachi) equipped with an energy-dispersive X-ray spectrum (EDS, JEOL JXA-840). The powder samples for EDS analysis were also completed to determine its elemental composition by increasing the accelerating voltage to 25 kV and reducing the working distance to 8.5 mm for an aperture of 30 μm. The EDX elemental composition was determined by comparing relative peak intensities together with the corresponding sensitivity factors of each element and assuming their total intensities to be 100%. Transmission electron microscopy (TEM) and high-resolution transmission electron microscopy (HRTEM) were performed on a FEI Tecnai G2 S-Twin transmission electron microscope with a field emission gun operating at 200 kV to elucidate the dimensions and the structural details of the particles. The photoluminescence (PL) excitation and emission spectra were recorded with a Hitachi F-7000 spectrophotometer equipped with a 150 W xenon lamp as the excitation source. The lifetime measurement was taken by using the third harmonic (355 nm) of a continuum Nd:YAG laser (pulse width = 4 ns, gate = 50 ns) with 5 mJ of energy per pulse as the source, and the emission lines were dispersed by the emission monochromator of the Acton Spectra Pro-2758 equipped with R928 PMT; the data were recorded by using a LeCroy Wave Runner 6100 digital oscilloscope (1 GHz). The luminescence lifetimes were calculated by the Origin 8.5 software package. All the measurements were performed at room temperature.

3. Results and discussion

3.1. Phase, structure and morphology

The composition and phase purity of the sodium lutetium fluoride with different RE^{3+} ions were first examined by XRD

 This journal is © The Royal Society of Chemistry 2012

Published on 13 June 2012. Downloaded on 21/01/2016 08:21:03.

measurement. Fig. 1 demonstrates the XRD patterns of as-prepared β-$NaLuF_4$:2.5% Eu^{3+}, $NaLuF_4$:2.5% Tb^{3+} and β-$NaLuF_4$:5% Ce^{3+}/2.5% Tb^{3+} samples. From all three patterns, it is obvious that these samples are highly crystalline, and the diffractions can be readily indexed to the pure β-$NaLuF_4$ phase (JCPDS No. 27-0726). No peaks from other phases or from doping are observed, indicating the high purity and that the Ce^{3+}, Eu^{3+} and Tb^{3+} ions have been effectively incorporated into the β-$NaLuF_4$ host by substituting Lu^{3+} sites. The calculated unit cell lattice constants corresponding to the lattice constants for the two samples are summarized in Table 1. It is found that these values from the crystalline samples are consistent with those from the standard card (JCPDS No. 27-0726). The slightly higher lattice constants may be caused by the larger ionic radius of the substituted Ce^{3+}, Eu^{3+} and Tb^{3+}. It should be noted that the markedly strengthened intensities of typical peaks may be caused by the preferred growth orientation of the samples.

Fig. 2 displays the FESEM, TEM and HRTEM images, and the EDS spectrum of the β-$NaLuF_4$ MCs prepared with an EG/EDA volume ratio of 3 : 17 at 200 °C for 24 h. It can be seen from Fig. 2a that β-$NaLuF_4$ exhibits a uniform six-sided prismatic structure with good monodispersity and a narrow size distribution. In the high magnification FESEM image (Fig. 2b), the prismatic structure has an average diameter of 1.94 μm and a thickness of 350 nm. The typical TEM image shows the obvious hexagonal microstructure with uniform size distribution (Fig. 2c). It should be noted that no chromatic aberration can be detected on the shadow part of the image, indicating the solid structure of the microplate. Besides, it is obvious that the surfaces on the top/bottom are very rough, which indicates an active growth on the surfaces under the conditions of relatively high temperature and pressure. A new side at the corresponding vertex of the hexagon can be found in the magnified TEM image (Fig. 2d), indicating active growth along the radial direction. The obvious lattice fringes in the HRTEM image (Fig. 2e) confirm the high crystallinity. The distance of 0.29 nm between the adjacent lattice fringes corresponds well to the d_{110} spacing of the hexagonal $NaLuF_4$ phase (JCPDS No. 27-0726). The EDS analysis (Fig. 2f) confirms the presence of Na, Lu, Ce, Tb and F, and the Na : (Lu + Ce + Tb) : F atomic ratio of 1 : 1.019 : 4.039 is in good agreement with the theoretical atomic Na : Lu : F ratio (1 : 1 : 4). The composition of the sample is further analysed by the ICP measurement; the respective quality percentage compositions of the Na^+, Lu^{3+}, Ce^{3+} and Tb^{3+} are 8.87, 60.35, 2.11, and 1.01 (corresponding molar ratios: 17.65%, 15.82%, 0.67%, and 0.31%, respectively), which agrees well with the EDS result and further confirms the composition of the $NaLuF_4$ crystals.

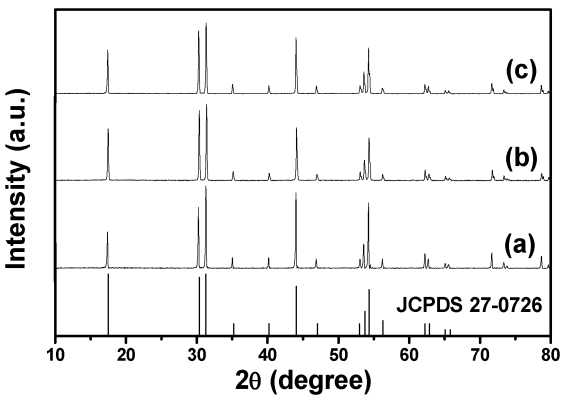

Fig. 1 XRD patterns of (a) β-$NaLuF_4$:2.5% Eu^{3+} MCs, (b) β-$NaLuF_4$:2.5% Tb^{3+} and (c) β-$NaLuF_4$:5% Ce^{3+}/2.5% Tb^{3+} MCs prepared with $NaNO_3$ content of 0.1 g at 200 °C for 24 h.

Table 1 Unit cell lattice constants for hexagonal β-$NaLuF_4$:2.5% Eu^{3+} MCs, hexagonal β-$NaLuF_4$:2.5% Tb^{3+} MCs and hexagonal β-$NaLuF_4$:5% Ce^{3+}/2.5% Tb^{3+} MCs

Samples	*a* (Å)	*c* (Å)	Cell volume (Å^3)
β-$NaLuF_4$:2.5% Eu^{3+}	5.914	3.448	104.45
β-$NaLuF_4$:2.5% Tb^{3+}	5.909	3.449	104.32
β-$NaLuF_4$:5% Ce^{3+}/2.5% Tb^{3+}	5.919	3.451	104.73
JCPDS No. 27-0726	5.901	3.453	104.13

3.2. Influential factors and possible formation mechanism

In the following sections, the effects of the EG/EDA volume ratio, $NaNO_3$ content and reaction time on the crystal structures and shapes of the final products are investigated in detail. Moreover, the possible formation mechanism for β-$NaLuF_4$ MCs with various morphologies is presented.

Effect of EG/EDA volume ratio. To investigate the effect of the EG/EDA volume ratio on the morphology of $NaLuF_4$ MCs, a series of contrasting experiments were conducted. Fig. 3 shows the FESEM images of β-$NaLuF_4$ MCs prepared with EG/EDA volume ratios of 0 : 20, 3 : 17, 7 : 13 and 10 : 10, respectively. In Fig. 3a, the crystals prepared with an EG/EDA volume ratio of 0 : 20 consist of regular and monodisperse hexagonal microplates with rough convex centers on the top/bottom surfaces. In the high magnification FESEM image (Fig. 3b), almost no side face can be discovered in the microplates and the mean diameter is 1.05 μm. Besides, some of the crystals are broken from the center, indicating that the microplates are relatively thin and only grow slightly along the axial direction. By contrast, the

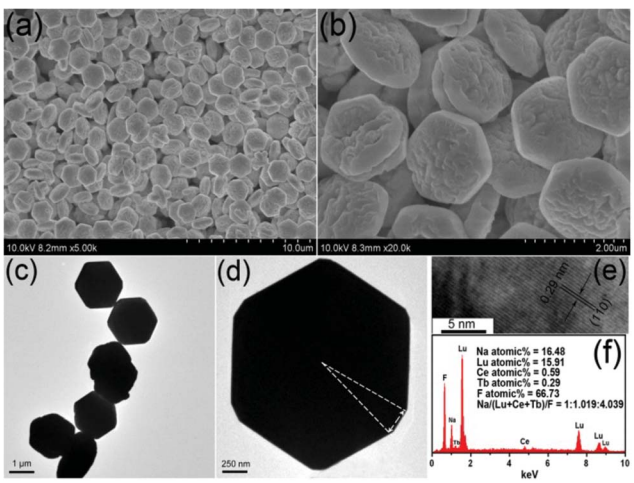

Fig. 2 Low- and high-magnification FESEM images (a) and (b), TEM images (c) and (d), HRTEM image (e), and EDS (f) of β-$NaLuF_4$ MCs prepared with $NaNO_3$ content of 0.1 g at 200 °C for 24 h.

Published on 13 June 2012. Downloaded on 21/01/2016 08:21:03.

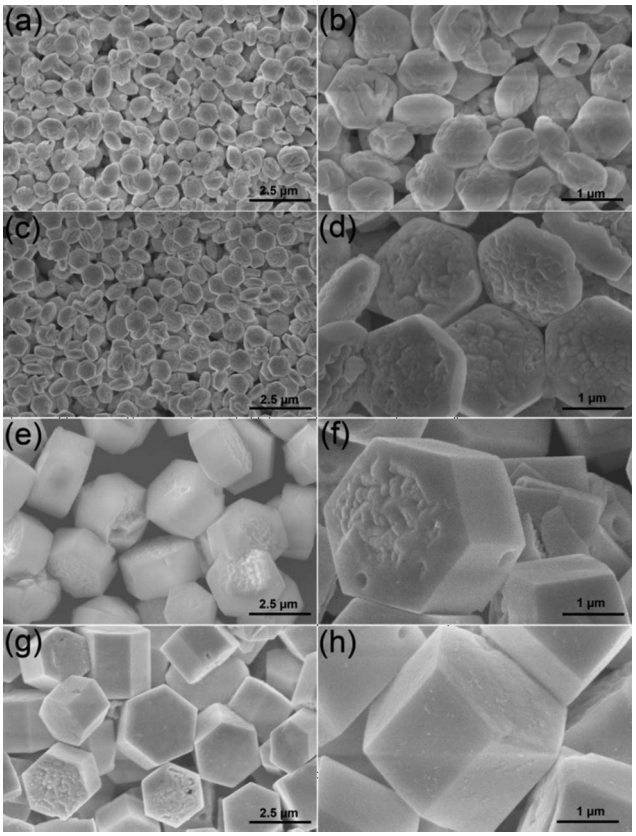

Fig. 3 Low- and high-magnification FESEM images of β-$NaLuF_4$ MCs prepared at 200 °C for 24 h and in EG/EDA volume ratios of 0 : 20 (a) and (b), 3 : 17 (c) and (d), 7 : 13 (e) and (f), 10 : 10 (g) and (h). All of the samples were obtained with $NaNO_3$ content of 0.1 g.

crystals synthesized with an EG/EDA volume ratio of 3 : 17 have further grown along the axial direction and the obvious side faces can be easily detected from Fig. 3c and Fig. 3d. Further increasing the EG/EDA volume ratio to 7 : 13, the crystal changes to a microprism structure with a diameter of 3.14 μm and a thickness of 1.55 μm, suggesting further growth along both the axial and radial directions (Fig. 3e). Furthermore, close observation (Fig. 3f) reveals that the top/bottom surface of the MCs changes to smooth from the fringe yet the center remains rough. When the EG/EDA volume ratio is enhanced to 10 : 10, the as-prepared products with a thickness of 2.78 μm exhibit further growth along the axial direction, while the average diameter is decreased to 2.85 μm compared with the last sample. On the basis of the above results, it can be inferred that the size of hexagonal β-$NaLuF_4$ MCs can be regulated by modulating the solvent constitution and increasing the EDA content can cause the structure to evolve from hexagonal microprism to hexagonal microplate. In fact, the capping effect and complexing ability of EDA have been proven by previous teams.[51–53] In the present system, EDA chelates with Lu^{3+} to form the $[Lu^{3+}(EDA)_m]^{3+}$ complex, which may decrease the quantity of free Lu^{3+} in the solution and strongly influence the crystal growth process, as shown in the following equations.[53]

$$Lu(NO_3)_3\ v{+}mEDA \leftrightarrow [Lu^{3+}(EDA)_m]^{3+}(complex) + 3NO_3^- \quad (1)$$

$$NaNO_3 \rightarrow Na^+ + NO_3^- \quad (2)$$

$$NH_4F \leftrightarrow NH_4^+ + F^- \quad (3)$$

$$Na^+ + [Lu^{3+}(EDA)_m]^{3+} + 4F^- \rightarrow NaLuF_4 + m\mathrm{EDA} \quad (4)$$

Besides, due to the anisotropy of the hexagonal β-$NaLuF_4$ structure, the EDA molecules can selectively adsorb on the typical {0001}, namely top/bottom surfaces, which are considered high surface energy and growth-active surfaces. When the EDA content in the solution is high, the strong capping effect on the top/bottom surfaces causes little growth along the axial direction of the crystals. Therefore, the crystals can grow more along the [1010] direction. However, owing to the low surface energy of the {1010} surfaces and the limited free Lu^{3+}, the growth rate on these surfaces is also quite low. So the hexagonal microplates can be obtained under these conditions. When the EDA content in the solution is relatively low, the capping effect and complexing ability of the EDA in the system will be reduced accordingly. As a result, the hexagonal microprisms with greater height and diameter can be synthesized.

In order to thoroughly investigate the effect of the solvent constitution on the morphology and structure, more widespread experiments have been carried out. Fig. 4 demonstrates the FESEM images of the products synthesized with EDA/EG volume ratios of 7 : 13, 3 : 17 and 0 : 20. In Fig. 4a and b, for the sample fabricated with an EDA/EG volume ratio of 7 : 13, the product comprises hexagonal microprisms with an average diameter of 1.87 μm and length of 3.52 μm. The remarkable structure transformation can also be explained by the mechanism proposed previously. Under the condition of lower EDA concentration, the crystals can grow more freely and quickly. Consequently, growth on the high energy {0001} surfaces can be promoted immensely and the hexagonal microprisms with high length/diameter ratios can be obtained. Interestingly, by further

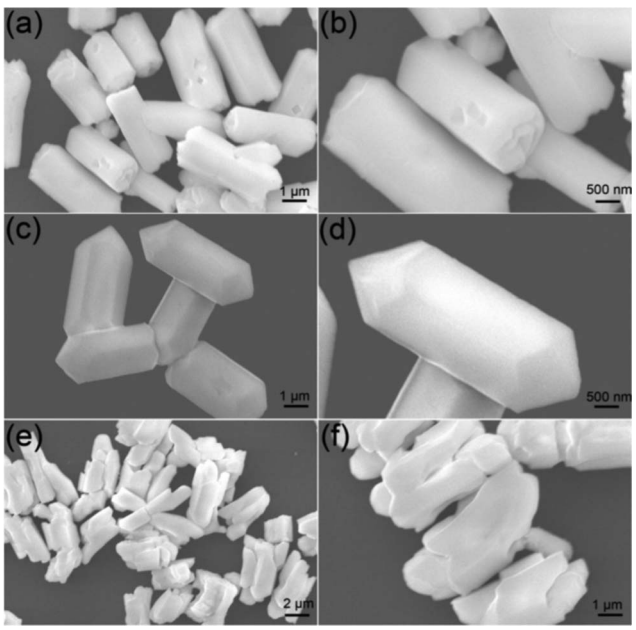

Fig. 4 Low- and high-magnification FESEM images of β-$NaLuF_4$ MCs prepared at 200 °C for 24 h and EDA/EG volume ratio of 7 : 13 (a) and (b), 3 : 17 (c) and (d), and 0 : 20 (e) and (f). All of the samples were obtained with $NaNO_3$ content of 0.1 g.

This journal is © The Royal Society of Chemistry 2012

Published on 13 June 2012. Downloaded on 21/01/2016 08:21:03.

increasing the EG content (EDA/EG volume ratio = 3 : 17), the uniform fusiform MCs with an average diameter of 1.96 μm and height of 5.31 μm can be achieved (Fig. 4c). Notably, the magnified image (Fig. 4d) shows that new surfaces have been created on the top/bottom surfaces, which suggests a speedy growth along the axial direction of the fusiform crystals. However, when pure EG was used as the solvent, only some irregular MCs could be found (Fig. 4e). In addition, the magnified image (Fig. 4f) indicates that the top/bottom surfaces of the MCs disappear, and are replaced by some tuber-like layers. The results reveal that EDA plays a very important role in the formation of the hexagonal β-$NaLuF_4$ MCs. By regulating the EDA content in the solvent, the microprisms with different heights and diameters can be obtained. In particular, the regulating process is effective, precise, and can be achieved easily.

Effect of $NaNO_3$ content. When the EDA/EG volume ratio was fixed at 10 : 10, 0.2, 0.3 and 0.4 g $NaNO_3$ were applied to investigate the effect of $NaNO_3$ content on the crystallization and morphology. When the $NaNO_3$ content in the initial solution is 5 mmol, the as-synthesized sample exhibits uniform hexagonal microprisms with the longer length of 3.54 μm and a similar diameter of 2.82 μm (Fig. 5a) than the product prepared with 2.5 mmol $NaNO_3$ (Fig. 3). The high-magnification FESEM image (Fig. 5b) indicates that concave centers on the top/bottom surfaces and a few micropores with diverse diameters are formed on the side surfaces. When more $NaNO_3$ (7.5 mmol) was added to the initial solution, uniform hexagonal microprisms with a longer mean length of 5.15 μm and an approximately equal mean diameter of 2.83 μm can be achieved (Fig. 5c). Moreover, close observation (Fig. 5d) shows that the microprisms with scraggly top/bottom surfaces have more serried micropores on the side surfaces, which means the formation of the rough side surfaces is in relation to the adding of $NaNO_3$. However, when the $NaNO_3$ content was further enhanced to 10 mmol, some irregular MCs with various diameters and lengths can be found and some of them are distorted, as shown in Fig. 5e and Fig. 5f. The mineralization of $NaNO_3$ has been proven by other groups previously.[54,55] When the superfluous $NaNO_3$ was added, it could act as a mineralizer and increase the chemical potential of the solution, which may lead to a dissolution–recrystallization process of β-$NaLuF_4$ into the stable phase with a bigger size,[56] which will be discussed in the following time-dependent experimental section. Besides, the micropores on the side surfaces may also be formed during this process. Simultaneously, some additional control experiments have been taken by using Na_2SO_4 and Na_3PO_4 as the sodium-source and mineralizer. It can be observed from the SEM and XRD results (Fig. S1†) that the as-prepared $NaLuF_4$ crystals are all inhomogenous in morphology, and the sample prepared with Na_2SO_4 is a mixed phase, which is possibly due to the low solubility of Na_2SO_4 and Na_3PO_4 in EG and EDA. In this work, regular microprisms with uniform size and micropore structure could only be obtained with suitable $NaNO_3$ content.

Effect of reaction time. Fig. 6 gives the XRD patterns and FESEM images of the samples prepared with reaction times of 1 h, 3 h and 6 h, respectively. In Fig. 6a, the XRD pattern of the sample prepared with a reaction time of 1 h (red line) shows some impure peaks according to the β-$NaLuF_4$ standard card (JCPDS No. 27-0726). The excrescent peaks can be assigned to the $Na_5Lu_9F_{32}$ phase (JCPDS No. 27-0725) by further analysis. When the reaction time is increased to 3 h, the intensities of the diffraction peaks (blue line) increase significantly compared with those in the red line (reaction time of 1 h), implying enhanced crystallinity. Furthermore, the diffraction peaks of the $Na_5Lu_9F_{32}$ phase are markedly degenerative compared with the sample prepared with a reaction time of 1 h, which indicates a phase transition and dissolution–recrystallization process.[57,58] By prolonging the reaction time to 6 h, the diffractions of the

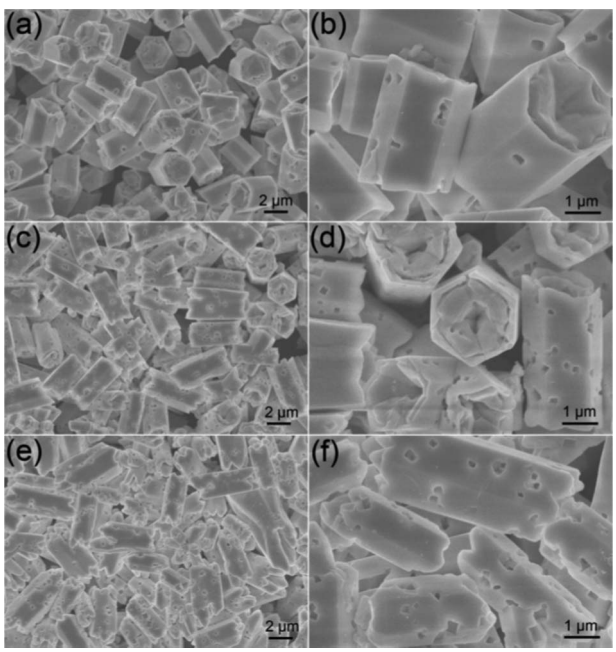

Fig. 5 Low- and high-magnification FESEM images of β-$NaLuF_4$ MCs synthesized at 200 °C for 24 h and differing $NaNO_3$ content of 5 mmol (a) and (b), 7.5 mmol (c) and (d), 10 mmol (e) and (f). All of the samples were obtained with an EDA/EG volume ratio of 10 : 10.

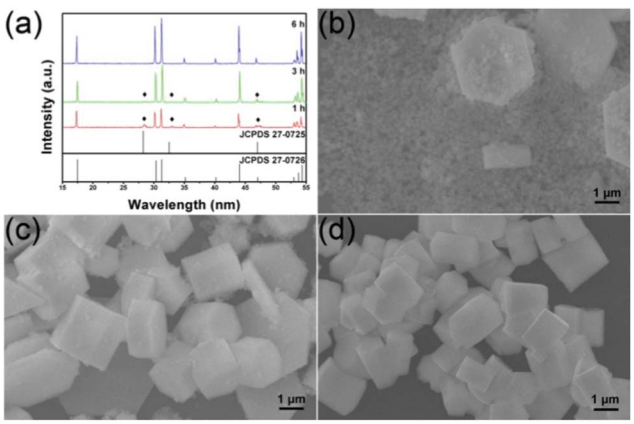

Fig. 6 XRD patterns (a) and FESEM images (b, c, d) of the β-$NaLuF_4$ MCs synthesized with differing reaction times of 1 h, 3 h and 6 h, respectively. All of the samples were obtained with an EDA/EG volume ratio of 10 : 10 and $NaNO_3$ content of 0.1 g.

Published on 13 June 2012. Downloaded on 21/01/2016 08:21:03.

as-prepared sample can be readily indexed to the pure β-$NaLuF_4$ phase (JCPDS No. 27-0726) and the intensities of the diffraction peaks increase greatly, suggesting a complete phase transition. The XRD results are well supported by the following FESEM images. In Fig. 6b for the sample fabricated with a reaction time of 1 h, two mixed structures composed of hexagonal micro-slices and many smaller particles can be observed, which may be associated with the mixed-phases of β-$NaLuF_4$ and $Na_5Lu_9F_{32}$, respectively. When the reaction time is prolonged to 3 h, the hexagonal microstructure becomes the dominant shape and only a few small particles can be found (Fig. 6c), which agrees well with the XRD results. The non-uniform size of the hexagonal microstructure may be due to the heterogeneous crystal growth with a deficient reaction time. With a reaction time of 6 h (Fig. 6d), no small particles ($Na_5Lu_9F_{32}$) can be found and the average size of the β-$NaLuF_4$ microstructures increases obviously compared to the last sample.

Possible formation mechanism. On the basis of the above analysis, it can be inferred that, besides the inherent unit cell structures of nucleated seeds, EG/EDA volume ratio, $NaNO_3$ content in the initial solution, and reaction times are all important factors in the phase and morphology evolution of the final crystals. Scheme 1 summarizes the possible morphology formation processes of sodium lutetium fluoride under various experimental conditions.

3.3. Luminescence properties of β-$NaLuF_4$:Ln^{3+} (Ln = Eu, Tb, Ce/Tb)

Our experimental results and previous investigations reveal that β-$NaLuF_4$ is a promising host lattice for doping optically active lanthanide ions.[40,41] Accordingly, we mainly focus on comparison of the down-conversion (DC) luminescence properties of β-$NaLuF_4$ MCs with different doping patterns of rare-earth ions, in an effort to show that our current solvothermal method is an efficient process for the synthesis of this kind of fluoride phosphor. All of the doping ratios of rare-earth ions are molar ratios in our experiments.

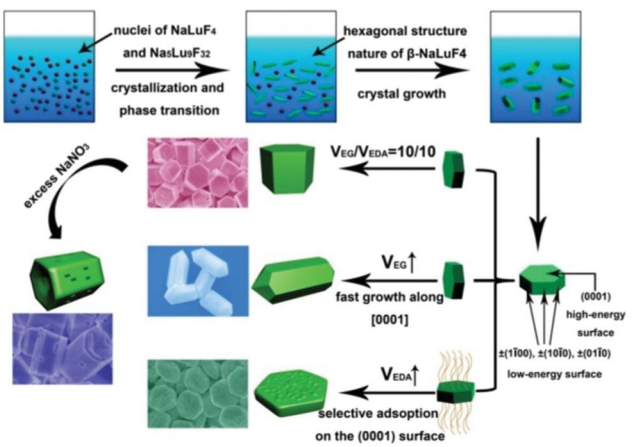

Scheme 1 Schematic illustration for the formation process of β-$NaLuF_4$ MCs prepared under different conditions.

β-$NaLuF_4$:2.5% Eu^{3+}. The excitation and emission spectra for the β-$NaLuF_4$:2.5% Eu^{3+} sample are shown in Fig. 7a. The excitation (left) and emission (right) spectra of β-$NaLuF_4$:2.5% Eu^{3+} shown in Fig. 7a are very similar to the previous report.[41] The excitation spectrum (black line) consists of several characteristic excitation lines of Eu^{3+} within its $4f^6$ configuration from 200 to 450 nm, which can be clearly assigned (318 nm, $^7F_0 \rightarrow {}^5H_6$; 363 nm, $F_0 \rightarrow {}^5D_4$; 382 nm, $^7F_0 \rightarrow {}^5G_2$; 397 nm, $^7F_0 \rightarrow {}^5L_6$, strongest; 418 nm, $^7F_0 \rightarrow {}^5D_3$), except for the weak ones at 255, 271, 289 and 301 nm (which contribute little to the excitation of Eu^{3+} and are of minor significance).[59] This is different from the excitation spectra for Eu^{3+} in oxide hosts in which a charge-transfer band (CTB) of Eu^{3+}–O^{2-} is frequently observed between 200 and 300 nm. The CTB of Eu^{3+}–F^- (generally located below 200 nm) is not present in this region because of the much greater energy needed to remove an electron from F^- than from O^{2-}.[60,61] Under excitation of the strongest $^7F_0 \rightarrow {}^5L_6$ transition of Eu^{3+} at 397 nm, the corresponding emission spectrum (red line) of β-$NaLuF_4$:2.5% Eu^{3+} comprises the emission lines associated with the Eu^{3+} transitions from the excited $^5D_{0,1,2}$ levels to the ^7F_J level, that is, $^5D_2 \rightarrow {}^7F_0$ (467 nm), $^5D_2 \rightarrow {}^7F_2$ (490 nm), $^5D_2 \rightarrow {}^7F_3$ (512 nm), $^5D_1 \rightarrow {}^7F_1$ (538 nm), $^5D_1 \rightarrow {}^7F_2$ (557 nm), $^5D_0 \rightarrow {}^7F_1$ (593 nm), $^5D_0 \rightarrow {}^7F_2$ (618 nm).[62–64] β-$NaLuF_4$:2.5% Tb^{3+} and β-$NaLuF_4$:5% Ce^{3+}/2.5% Tb^{3+}. The β-$NaLuF_4$:2.5% Tb^{3+} and β-$NaLuF_4$:5% Ce^{3+}/2.5% Tb^{3+} samples emit a bright-green light under UV excitation. Fig. 7b shows the excitation (left) and emission (right) spectra of the samples. For β-$NaLuF_4$:2.5% Tb^{3+}, similarly to the Eu^{3+} complex, the excitation spectrum (black line in bottom of Fig. 7b) is composed

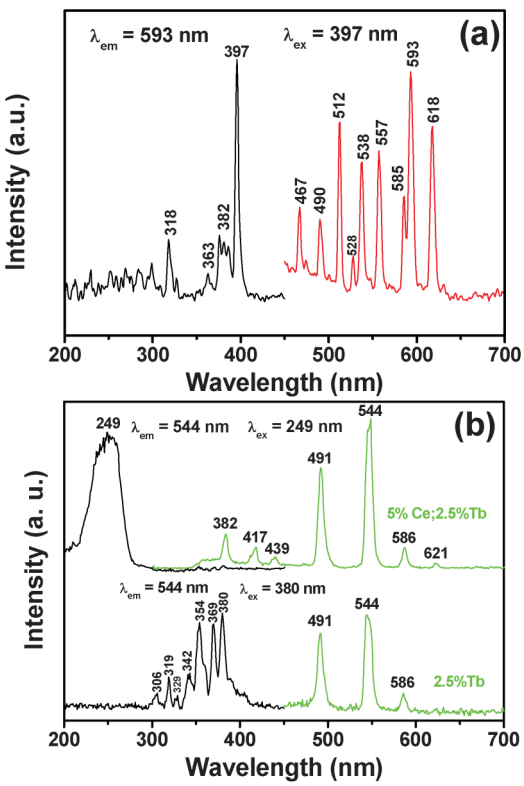

Fig. 7 Excitation (black lines) and emission spectra (red/green lines) of β-$NaLuF_4$:2.5% Eu^{3+} (Fig. 7a), β-$NaLuF_4$:2.5% Tb^{3+} (bottom of Fig. 7b) and β-$NaLuF_4$:5% Ce^{3+}/2.5% Tb^{3+} (top of Fig. 7b).

This journal is © The Royal Society of Chemistry 2012

Published on 13 June 2012. Downloaded on 21/01/2016 08:21:03.

of the characteristic f–f transition lines within the Tb^{3+} $4f^8$ configuration, which can be assigned to the transitions from the $^7F_6$ ground state to the different excited states of Tb^{3+}, that is, 288 nm ($^5I_6$), 306 nm ($^5H_6$), 321 nm ($^5D_0$), 344 nm ($^5G_2$), 356 nm ($^5D_2$), and 372 nm ($^5G_6$).[65,66] Upon excitation into the $^7F_6 \rightarrow {}^5D_2$ transition at 380 nm, the obtained emission spectrum consists of three obvious lines centered at 491, 544 and 586 nm, originating from the transitions from the $^5D_4$ excited state to the ^7F_J (J = 6, 5, 4) ground states of the Tb^{3+} ions, respectively (green line in bottom of Fig. 7b).[67–69] And the $^5D_4 \rightarrow {}^7F_5$ transition at 544 nm is the most intense group. Dramatically, when co-doping 5% Ce^{3+} with 2.5% Tb^{3+} into β-$NaLuF_4$ MCs, dramatic changes took place in the excitation and emission spectra. Firstly, in the excitation spectrum, a broad absorption band at around 249 nm was observed (black line in top of Fig. 7b), instead of several absorption peaks in the excitation spectrum of β-$NaLuF_4$:2.5% Tb^{3+}. This indicates that the method of energy absorption has completely changed to the characteristic 4f–5d transition of Ce^{3+}. Consequently, the corresponding emission spectrum has been strengthened obviously (green line in top of Fig. 7b). Additionally, the new emission peaks located at 382, 417, 439 and 621 nm appear, which are generated from the 4f–4f transition of the Tb^{3+} ion of $^5D_3 \rightarrow {}^7F_6$, $^5D_3 \rightarrow {}^7F_5$, $^5D_3 \rightarrow {}^7F_4$, and $^5D_4 \rightarrow {}^7F_3$, respectively. The proposed down-conversion mechanism in β-$NaLuF_4$:Ce^{3+}/Tb^{3+} MCs is demonstrated in Fig. 8.

In order to further investigate the luminescence properties of β-$NaLuF_4$ MCs, samples with different Ce^{3+} doping concentrations were prepared by fixing the Tb^{3+} concentration at 2.5%. Fig. 9 shows the emission spectra of β-$NaLuF_4$:Ce^{3+}/Tb^{3+} with four Ce^{3+} concentrations of 2.5% Ce^{3+}/2.5% Tb^{3+}, 5% Ce^{3+}/2.5% Tb^{3+}, 7.5% Ce^{3+}/2.5% Tb^{3+} and 10% Ce^{3+}/2.5% Tb^{3+}, respectively. It can be seen that the emission intensity increases with increasing Ce^{3+} concentration from 2.5% to 5%, and then decreases with further increase in Ce^{3+} concentration, which indicates that β-$NaLuF_4$:5% Ce^{3+}/2.5% Tb^{3+} MCs have the highest emission intensity. A possible interpretation is proposed as follows. When the Ce^{3+} concentration increases from 2.5% to 5%, more Ce ions become available to furnish and transfer the energy to the Tb^{3+}, resulting in the higher emission intensity. When the Ce^{3+} concentration is further raised, the cross-relaxation process for the superfluous Ce^{3+} ions leads to the decrease in emission intensity. With the additional increase in Ce^{3+} concentration, the distance between neighbouring Ce^{3+} ions becomes shorter, which can enhance the interaction of the neighbouring Ce^{3+} ions and intensify the cross-relaxation process of Tb ions, thus resulting in concentration-dependent quenching.

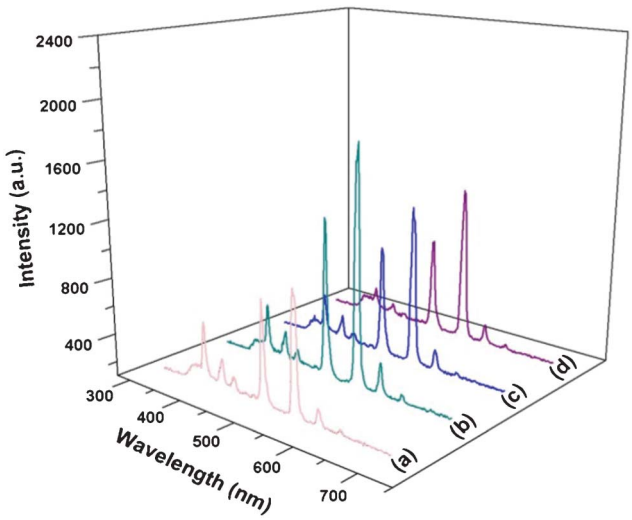

Fig. 9 Emission spectra of β-$NaLuF_4$ MCs with doping concentrations of 2.5% Ce^{3+}/2.5% Tb^{3+} (a), 5% Ce^{3+}/2.5% Tb^{3+} (b), 7.5% Ce^{3+}/2.5% Tb^{3+} (c), and 10% Ce^{3+}/2.5% Tb^{3+} (d).

The PL decay curve for the luminescence of β-$NaLuF_4$:5% Ce^{3+}/2.5% Tb is depicted in Fig. 10. This curve can be well fitted by a single exponential function as $I(t) = I_0 \exp(-t/\tau)$ (I_0 is the initial emission intensity at t = 0, τ is the 1/e lifetime of the emission center), and the Tb^{3+} ($^5D_4 \rightarrow {}^7F_5$, detected at 544 nm) were determined to be 0.72 and 0.47 ms, respectively.

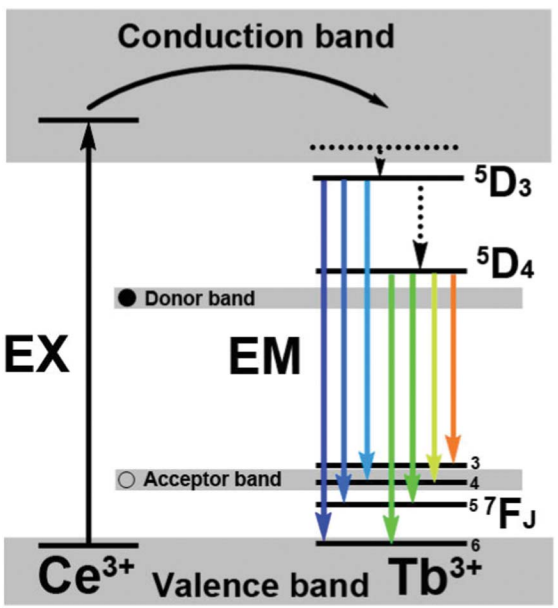

Fig. 8 The energy transfer mechanisms in β-$NaLuF_4$:Ce^{3+}/Tb^{3+} MCs.

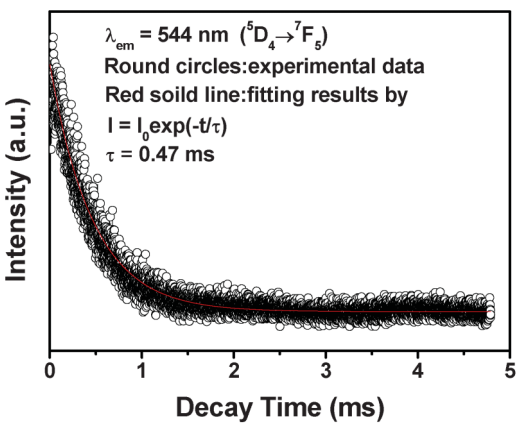

Fig. 10 Decay curve for the $^5D_4 \rightarrow {}^7F_5$ emission of Tb^{3+} in β-$NaLuF_4$:5% Ce^{3+}/2.5% Tb^{3+}.

View Article Online

Published on 13 June 2012. Downloaded on 21/01/2016 08:21:03.

4. Conclusions

In summary, β-$NaLuF_4$ MCs were synthesized through a mild and manageable solvothermal method by using EDA and EG as the mixed solvent and $NaNO_3$ as the mineralizer. The results indicate that the solvent constitution has a significant role in the morphology, dimension and structure of the products. Besides, the dissolution–recrystallization process introduced by adding excess $NaNO_3$ gives rise to a bigger size and micropore structure of the β-$NaLuF_4$ MCs. Time-dependent experiments convincingly support the proposed analyses. The possible formation mechanisms for β-$NaLuF_4$ MCs with diverse morphologies were presented in detail. Furthermore, co-doped Eu^{3+}, Tb^{3+}, and Ce^{3+} exhibit characteristic emission properties in the β-$NaLuF_4$ MCs host, which bring effective improvement of the luminescence properties. Particularly, the DC luminescence properties of β-$NaLuF_4$ can be obviously improved by co-doped Ce with Tb, which can be popularized to other $NaREF_4$ materials. The products with peculiar characteristics may have the promising potential to serve as versatile luminescent phosphors in further applications.

Acknowledgements

Financially supported from Research Fund for the Doctoral Program of Higher Education of China (20112304110021), Harbin Sci.-Tech. Innovation Foundation (RC2012XK017012) and the Fundamental Research Funds for the Central Universities of China are greatly acknowledged.

References

1 A. Umemura, S. Diring, S. Furukawa, H. Uehara, T. Tsuruoka and S. Kitagawa, *J. Am. Chem. Soc.*, 2011, **133**, 15506.
2 F.-R. Fan, Y. Ding, D.-Y. Liu, Z.-Q. Tian and Z. L. Wang, *J. Am. Chem. Soc.*, 2009, **131**, 12036.
3 Y. Xiong, H. Cai, B. J. Wiley, J. Wang, M. J. Kim and Y. Xia, *J. Am. Chem. Soc.*, 2007, **129**, 3665.
4 D. Tu, L. Liu, Q. Ju, Y. Liu, H. Zhu, R. Li and X. Chen, *Angew. Chem., Int. Ed.*, 2011, **50**, 6306.
5 Y. Dai, P. Ma, Z. Cheng, X. Kang, X. Zhang, Z. Hou, C. Li, D. Yang, X. Zhai and J. Lin, *ACS Nano*, 2012, **6**, 3327.
6 D. Shi, H. S. Cho, Y. Chen, H. Xu, H. Gu, J. Lian, W. Wang, G. Liu, C. Huth, L. Wang, R. C. Ewing, S. Budko, G. M. Pauletti and Z. Dong, *Adv. Mater.*, 2009, **21**, 2170.
7 B. Lee, S. Lee, H. G. Jeong and K.-S. Sohn, *ACS Comb. Sci.*, 2011, **13**, 154.
8 W. B. Park, S. P. Singh, M. Pyo and K.-S. Sohn, *J. Mater. Chem.*, 2011, **21**, 5780.
9 Z. Cai, X. Xing, R. Yu and X. Sun, *Inorg. Chem.*, 2007, **46**, 7423.
10 Y. Wang, Y. Liu, Q. Xiao, H. Zhu, R. Li and X. Chen, *Nanoscale*, 2011, **3**, 3164.
11 D.-P. Li, Z. Zheng, Y. Lei, F.-L. Yang, S.-X. Ge, Y.-D. Zhang, B.-J. Huang, Y.-H. Gao, K.-W. Wong and W.-M. Lau, *Chem.–Eur. J.*, 2011, **17**, 7694.
12 C. Zhang, C. Li, C. Peng, R. Chai, S. Huang, D. Yang, Z. Cheng and J. Lin, *Chem. Eur. J.*, 2010, **16**, 5672.
13 P. Tonto, O. Mekasuwandumrong, S. Phatanasri, V. Pavarajarn and P. Praserthdam, *Ceram. Int.*, 2008, **34**, 57.
14 G. Li, C. Peng, C. Zhang, Z. Xu, M. Shang, D. Yang, X. Kang, W. Wang, C. Li, Z. Cheng and J. Lin, *Inorg. Chem.*, 2010, **49**, 10522.
15 B. Yang, P. R. F. Barnes, W. Bertram and V. Luca, *J. Mater. Chem.*, 2007, **17**, 2722.
16 J. Ge and Y. Li, *Adv. Funct. Mater.*, 2004, **14**, 157.
17 Z. Wang, J. Hao and H. Chan, *J. Mater. Chem.*, 2010, **20**, 3178.
18 X. Gou, F. Cheng, Y. Shi, L. Zhang, S. Peng, J. Chen and P. Shen, *J. Am. Chem. Soc.*, 2006, **128**, 7222.
19 Z. Li, J. Zeng and Y. Li, *Small*, 2007, **3**, 438.
20 J. Hao, Y. Zhang and X. Wei, *Angew. Chem., Int. Ed.*, 2011, **50**, 6876.
21 N. Chouhan, C. L. Yeh, S.-F. Hu, R.-S. Liu, W.-S. Chang and K.-H. Chen, *Chem. Commun.*, 2011, **47**, 3493.
22 Z. Liu, S. Peng, Q. Xie, Z. Hu, Y. Yang, S. Zhang and Y. Qian, *Adv. Mater.*, 2003, **15**, 936.
23 H. Yang, G. Liu, S. Qiao, C. Sun, Y. Jin, S. Smith, J. Zou, H. Cheng and G. Lu, *J. Am. Chem. Soc.*, 2009, **131**, 4078.
24 H. Wang, J. Robinson, X. Li and H. Dai, *J. Am. Chem. Soc.*, 2009, **131**, 9910.
25 W. Yin, J. Su, M. Cao, C. Ni, C. Hu and B. Wei, *J. Phys. Chem. C*, 2009, **114**, 65.
26 L.-P. Zhu, H.-M. Xiao, W.-D. Zhang, G. Yang and S.-Y. Fu, *Cryst. Growth Des.*, 2008, **8**, 957.
27 H.-S. Cho, Z. Dong, G. M. Pauletti, J. Zhang, H. Xu, H. Gu, L. Wang, R. C. Ewing, C. Huth, F. Wang and D. Shi, *ACS Nano*, 2010, **4**, 5398.
28 X. Ye, J. E. Collins, Y. Kang, J. Chen, D. T. N. Chen, A. G. Yodh and C. B. Murray, *Proc. Natl. Acad. Sci. U. S. A.*, 2010, **107**, 22430.
29 F. Zhang, Y. Wan, Y. Shi, B. Tu and D. Zhao, *Chem. Mater.*, 2008, **20**, 3778.
30 Y. I. Park, J. H. Kim, K. T. Lee, K. S. Jeon, H. B. Na, J. H. Yu, H. M. Kim, N. Lee, S. H. Choi, S. I. Baik, H. Kim, S. P. Park, B. J. Park, Y. W. Kim, S. H. Lee, S. Y. Yoon, I. C. Song, W. K. Moon, Y. D. Suh and T. Hyeon, *Adv. Mater.*, 2009, **21**, 4467.
31 R.-S. Liu, Y.-H. Liu, N. C. Bagkar and S.-F. Hu, *Appl. Phys. Lett.*, 2007, **91**, 61119.
32 S. R. Ghosh, T. F. Aeppli and G. Coppersmith, S. N., *Nature*, 2003, **425**, 48.
33 T.-C. Liu, B.-M. Cheng, S.-F. Hu and R.-S. Liu, *Chem. Mater.*, 2011, **23**, 3698.
34 E. Downing, L. Hesselink, J. Ralston and R. Macfarlane, *Science*, 1996, **273**, 1185.
35 C. Lin and R.-S. Liu, *J. Phys. Chem. Lett.*, 2011, **2**, 1268.
36 G. Yi, H. Lu, S. Zhao, G. Yue, W. Yang, D. Chen and L. Guo, *Nano Lett.*, 2004, **4**, 2191.
37 L. Wang and Y. Li, *Chem. Commun.*, 2006, **24**, 2557.
38 Z. Hou, C. Li, P. Ma, G. Li, Z. Cheng, C. Peng, D. Yang, P. Yang and J. Lin, *Adv. Funct. Mater.*, 2011, **21**, 2356.
39 F. Vetrone, R. Naccache, A. Zamarrón, A. Juarranz de la Fuente, F. Sanz-Rodríguez, L. Martinez Maestro, E. Martiín Rodriguez, D. Jaque, J. García Solí and J. A. Capobianco, *ACS Nano*, 2010, **4**, 3254.
40 T. Chan, C. Dong, Y. Chen, Y. Lu, S. Wu, Y. Ma, C. Lin, R. Liu, J. Chen, J. Guo, J. Lee, H. Sheu, C. Yang and C. Chen, *J. Mater. Chem.*, 2011, **21**, 17119.
41 C. Li, J. Yang, P. Yang, X. Zhang, H. Lian and J. Lin, *Cryst. Growth Des.*, 2008, **8**, 923.
42 O. Guillot-Noël, B. Bellamy, B. Viana and D. Vivien, *Phys. Rev. B: Condens. Matter*, 1999, **60**, 1668.
43 J. A. Capobianco, F. Vetrone, J. C. Boyer, A. Speghini and M. Bettinelli, *Opt. Mater.*, 2002, **19**, 259.
44 D. Chen, Y. Wang and F. Weng, *J. Phys. Chem. C*, 2009, **113**, 6406.
45 M. Laroche, S. Girard, R. Moncorgé, M. Bettinelli, R. Abdulsabirov and V. Semashko, *Opt. Mater.*, 2003, **22**, 147.
46 F. Zhang, Y. Shi, X. Sun, D. Zhao and G. Stucky, *Chem. Mater.*, 2009, **21**, 5237.
47 D. Yang, X. Kang, M. Shang, G. Li, C. peng, C. Li and J. Lin, *Nanoscale*, 2011, **3**, 2589.
48 S. Nigam, V. Sudarsan, R. K. Vatsa, J. Ghattak and P. V. Satyam, *J. Phys. Chem. C*, 2009, **113**, 8750.
49 Y. Huang, H. You, G. Jia, Y. Song, Y. Zheng, M. Yang, K. Liu and N. Guo, *J. Phys. Chem. C*, 2010, **114**, 18051.
50 J.-W. Lee, J.-H. Lee, E.-J. Woo, H. Ahn, J.-S. Kim and C.-H. Lee, *Ind. Eng. Chem. Res.*, 2008, **47**, 5994.
51 S. Kar, C. Patel and S. Santra, *J. Phys. Chem. C*, 2009, **113**, 4862.
52 F. Lu, W. P. Cai and Y. G. Zhang, *Adv. Funct. Mater.*, 2008, **18**, 1047.
53 J. Jang, U. Joshi and J. S. Lee, *J. Phys. Chem. C*, 2007, **111**, 13280.
54 W. Liu, N. Wang, R. Wang, S. Kumar, G. Duesberg, H. Zhang and K. Sun, *Nano Lett.*, 2011, **11**, 2983.
55 X. Qu, H. Yang, G. Pan, J. W. Chung, B. Moon, B. Choi and J. H. Jeong, *Inorg. Chem.*, 2011, **50**, 3387.
56 R. Qin, H. Song, G. Pan, X. Bai, B. Dong, S. Xie, L. Liu, Q. Dai, X. Qu, X. Ren and H. Zhao, *Cryst. Growth Des.*, 2009, **9**, 1750.

 This journal is © The Royal Society of Chemistry 2012

View Article Online

57 X. Hu, Y. Masuda, T. Ohji and K. Kato, *Cryst. Growth Des.*, 2009, **10**, 626.
58 G. Xi, K. Xiong, Q. Zhao, R. Zhang, H. Zhang and Y. Qian, *Cryst. Growth Des.*, 2006, **6**, 577.
59 J. B. Liang, J. W. Liu, Q. Xie, S. Bai, W. C. Yu and Y. T. Qian, *J. Phys. Chem. B*, 2005, **109**, 9436.
60 L. G. Deshazer and G. H. Dieke, *J. Chem. Phys.*, 1963, **38**, 2190.
61 J. C. Krupa and M. J. Queffelec, *J. Alloys Compd.*, 1997, **250**, 287.
62 M. Yu, J. Lin and J. Fang, *Chem. Mater.*, 2005, **17**, 1783.
63 Y. Liu, D. Tu, H. Zhu, R. Li, W. Luo and X. Chen, *Adv. Mater.*, 2010, **22**, 3266.
64 Y. Wang, Y. Liu, Q. Xiao, H. Zhu, R. Li and X. Chen, *Nanoscale*, 2011, **3**, 3164.
65 M. Yang, H. You, K. Liu, Y. Zheng, N. Guo and H. Zhang, *Inorg. Chem.*, 2010, **49**, 4996.
66 L. Yu, H. Song, Z. Liu, L. Yang and S. L. Z. Zheng, *J. Phys. Chem. B*, 2005, **109**, 11450.
67 Z. Wang, Z. Quan, P. Jia, C. Lin, Y. Luo, Y. Chen, J. Fang, W. Zhou, C. O'Connor and J. Lin, *Chem. Mater.*, 2006, **18**, 2030.
68 Z. Wang, Z. Quan, J. Lin and J. Fang, *J. Nanosci. Nanotech.*, 2005, **5**, 1523.
69 C. Li and J. Lin, *J. Mater. Chem.*, 2010, **20**, 6831–6847.

Published on 13 June 2012. Downloaded on 21/01/2016 08:21:03.